CONEM 2016
CONGRESSO NACIONAL DE ENGENHARIA MECÂNICA
21 - 25 AGOSTO DE 2016
FORTALEZA - CEARÁ

HOVERING ANALYSIS OF A TETHERED MULTIROTOR UNDER EXTERNAL DISTURBANCES

CON-2016-1210

Abstract: *Multirotor Aerial Vehicles (MAVs) have been the subject of many academic studies and have attracted a lot of attention from industry in recent years. MAVs have flight capabilities such as hovering, Vertical Take-Off and Landing (VTOL) and agile maneuvering capability, which cannot be achieved by conventional fixed wing aircraft. However, such vehicles have limited autonomy, which results in flights of at most some minutes. A sub-category of aerial vehicles is tethered MAVs, which are anchored at a fixed point by a cable. While this limits their motion, it can also works as a power line, providing electrical power to the vehicle and enhancing its flight autonomy. This paper presents a modeling and hovering control strategy for tethered MAV. The vehicle is an octocopter, with flat configuration. A viscoelastic model is considered for the cable, in order to reproduce its dynamic behavior. The cable consists of a spring and a damper in parallel. The controller is based on a saturated state feedback control, thus simplifying the controller. The model was evaluated through numerical simulations using MATLAB/Simulink. The vehicle performed a hover flight and was subjected to external disturbances in order to emulate ambient wind. The results for the tethered MAV were compared with the MAV flying freely without cable. The tethered MAV presents improved hovering capability when compared with the vehicle without cable, due to the tension exerted by the cable, which provides a better robustness to exogenous perturbations.*

Keywords: *Multirotor Aerial Vehicles, Tethered Multirotor, Modeling.*

1. INTRODUCTION

Multirotor Aerial Vehicles (MAVs) have been the subject of many academic studies and have attracted a lot of attention from industry in recent years. MAVs have flight capabilities such as hovering, Vertical Take-Off and Landing (VTOL) and agile maneuvering capability, which cannot be achieved by conventional fixed wing aircraft. Some drawbacks of multicopter vehicles are the reduced endurance, which hardly exceeds some minutes and limited payload. Tethered MAVs have been introduced to the aerospace sector as a possible alternative. The tether, even though limiting the vehicle flight range, can be used for data transmission and power supply during operation, which improves the vehicle endurance.

The capability of quickly reaching high altitudes for communication and surveillance operations is crucial for a variety of missions. Therefore, tethered multicopters would take over a niche that fixed-wing UAVs[1] and tethered aerostats cannot fulfill currently. Incidentally, tethered multicopters are easily set up and are able to operate in an efficient way for long periods at altitudes of some meters above the ground, with no halt in data transmission, which flows through the cable. Moreover, electronic equipment such as radars, antennas and cameras can be added to the vehicle.

In academia, research works on tethered multicopters are still rare by the present day and there are few companies and institutions that have invested in the development of such vehicles. The first references to consider the tethered configuration are found in Schmidt and Swik (1974) and Rye (1985). Some applications of this kind configuration are found in aerostats Khaleefa *et al.* (2014) and robot satellites Nohmi (2009). The work in Papachristos and Tzes (2014) presents a navigation strategy in partially mapped environments. This strategy is applied to the collaboration between an UAV and an UGV [2], in which power is provided to the former by a cable connecting the two vehicles. The work Sandino *et al.* (2014) presents a control strategy for tethered helicopters in hover and a model for the tether in which viscosity is taken into consideration, where the authors use a combination of classical PID control laws. The use of the cable tension in the tethered configuration for improving the stability at hover under disturbances is still a topic not deeply explored in the literature. The works related to this topic are only Sandino *et al.* (2013b) and Sandino *et al.* (2013a). Another topic of research is modeling and control as presented in Castro *et al.* (2015) and Castro *et al.* (2016).

This paper presents a modeling and position control strategy for tethered MAV. A viscoelastic model is considered for the cable, in order to reproduce its dynamic behavior. The controller is based on a saturated state feedback control, thus simplifying the controller. This paper is organized as follows: in Section 2 we present the tethered configuration

[1] Unmanned Aerial Vehicle (UAV)
[2] Unmanned Ground Vehicle (UGV)

model, in Section 3 a control system is proposed, in Section 4 we present the simulation results and Section 5 presents the conclusions.

2. TETHERED CONFIGURATION MODEL

This Section presents the multicopter model and tether model, which together describe the dynamics of the tethered multicopter configuration.

2.1 Multicopter Model

Consider a octocopter and four Cartesian coordinate systems (CCS) illustrated in Fig. 1.

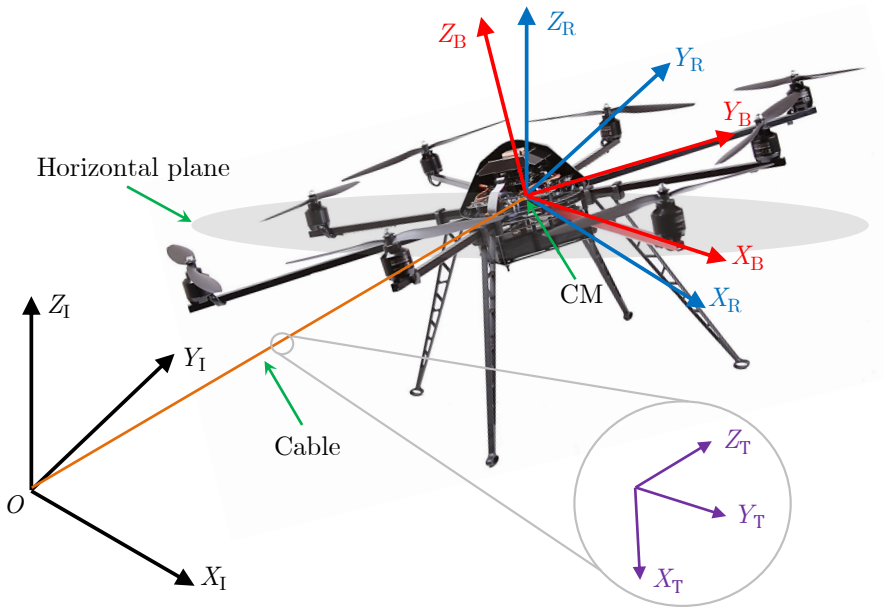

Figura 1: Cartesian coordinate systems.

The CCS of the body $S_B \triangleq \{X_B,\ Y_B,\ Z_B\}$ is fixed to the vehicle structure and centered on the center of mass (CM). The inertial CCS $S_I \triangleq \{X_I,\ Y_I,\ Z_I\}$ is fixed to the earth at the point O. The CCS $S_R \triangleq \{X_R,\ Y_R,\ Z_R\}$ is parallel to S_I and centered in CM. The CCS of the tether $S_T \triangleq \{X_T,\ Y_T,\ Z_T\}$ is fixed to the cable structure.

The differential equations that describe the dynamic behavior of the multirotor can be obtained by the Newton-Euler formalism. This work chooses to represent the attitude by the quaternion of rotation $\mathbf{q} \in \mathbb{R}^4$, however for visualization is adopted Euler angles (ϕ, θ and ψ).

The kinematic attitude model for the quaternion of rotation is given by the following differential equation Wertz (1978):

$$\dot{\mathbf{q}} = \mathbf{\Omega q} \tag{1}$$

where

$$\mathbf{\Omega} = \frac{1}{2}\begin{bmatrix} 0 & -\boldsymbol{\omega}^{\mathrm{T}} \\ \boldsymbol{\omega} & -[\boldsymbol{\omega}\times] \end{bmatrix}, \tag{2}$$

being $\boldsymbol{\omega} \triangleq [\omega_x\ \omega_y\ \omega_z]^{\mathrm{T}} \in \mathbb{R}^3$ the angular velocity of the vehicle represented in S_R and $[\boldsymbol{\omega}\times]$ is given by:

$$[\boldsymbol{\omega}\times] = \begin{bmatrix} 0 & -\omega_z & \omega_y \\ \omega_z & 0 & -\omega_x \\ -\omega_y & \omega_x & 0 \end{bmatrix}. \tag{3}$$

Rewriting the equation (1) explicitly, one obtains:

$$\begin{bmatrix} \dot{q}_1 \\ \dot{q}_2 \\ \dot{q}_3 \\ \dot{q}_4 \end{bmatrix} = \frac{1}{2}\begin{bmatrix} 0 & -\omega_x & -\omega_y & -\omega_z \\ \omega_x & 0 & \omega_z & -\omega_y \\ \omega_y & -\omega_z & 0 & \omega_x \\ \omega_z & \omega_y & -\omega_x & 0 \end{bmatrix}\begin{bmatrix} q_1 \\ q_2 \\ q_3 \\ q_4 \end{bmatrix}. \tag{4}$$

Applying Newton's second law for rotational motion and neglecting disturbance torques, one can obtain:

$$\boldsymbol{\tau} = \dot{\mathbf{h}} + \boldsymbol{\omega} \times \mathbf{h}, \tag{5}$$

where $\boldsymbol{\tau} \triangleq [\tau_x\ \tau_y\ \tau_z]^{\mathrm{T}} \in \mathbb{R}^3$ is the resulting propulsion torque in the vehicle represented in S_{B} and $\mathbf{h} \triangleq \mathbf{I}\,\boldsymbol{\omega} \in \mathbb{R}^3$ is the angular momentum of the body represented in S_{B}, being $\mathbf{I} \in \mathbb{R}^{3x3}$ the matrix of inertia of the vehicle represented in S_{B}. It is assumed that the vehicle has symmetrical structure with respect to the coordinate axes. The matrix $\mathbf{I}$ resulting in a diagonal matrix defined by:

$$\mathbf{I} = \begin{bmatrix} I_x & 0 & 0 \\ 0 & I_y & 0 \\ 0 & 0 & I_z \end{bmatrix}. \tag{6}$$

Rewriting the equation (5) explicitly, one can obtain:

$$\dot{\omega}_x = \frac{(I_y - I_z)}{I_x}\omega_y\omega_z + \frac{\tau_x}{I_x}. \tag{7}$$

$$\dot{\omega}_y = \frac{(I_z - I_x)}{I_y}\omega_x\omega_z + \frac{\tau_y}{I_y}. \tag{8}$$

$$\dot{\omega}_z = \frac{(I_x - I_y)}{I_z}\omega_x\omega_y + \frac{\tau_z}{I_z}. \tag{9}$$

Applying the second Newton's law of motion, we obtain the following model of translational movement in S_{I}:

$$\ddot{\mathbf{r}} = \frac{1}{m} f\mathbf{n} + \begin{bmatrix} 0 \\ 0 \\ -g \end{bmatrix} + \mathbf{D}_{\mathrm{I}} + \mathbf{F}_{\mathrm{T}}, \tag{10}$$

where $\mathbf{r} \triangleq [r_x\ r_y\ r_z]^{\mathrm{T}} \in \mathbb{R}^3$ is the three-dimensional position of the CM represented in S_{I}, $\mathbf{n} \triangleq [n_x\ n_y\ n_z]^{\mathrm{T}} \in \mathbb{R}^3$ is the normal unit vector perpendicular to the rotor plane represented in S_{I}, f is the total thrust, g is the acceleration of gravity, m is the mass of the vehicle, $\mathbf{D}_{\mathrm{I}} \triangleq [D_{X_I}\ 0\ 0]^{\mathrm{T}} \in \mathbb{R}^3$ is the drag force and $\mathbf{F}_{\mathrm{T}}$ is the force from the tether. The drag force component is given by:

$$D_{X_{\mathrm{I}}} = \frac{1}{2}\rho_{air} C_d A_o |\dot{r}_a|^2 \tag{11}$$

where ρ_{air} is the air density, C_d is the drag coefficient, A_o is the octocopter section area and $\dot{r}_a$ is the relative velocity between the wind and the center of mass of the vehicle. These parameters are shown in Table 1.

Tabela 1: Parameters of the octocopter.

	Parameter	Value	Units
Mass	m	2.132	Kg
Gravity acceleration	g	9.796	m/s^2
Section area	A_o	0.0185	m^2
Drag coefficient	C_d	0.98	
Inertia component in X	I_x	0.0628	[Kg/m^2]
Inertia component in Y	I_y	0.0762	[Kg/m^2]
Inertia component in Z	I_z	0.1014	[Kg/m^2]

2.2 Tether Model

The tether model was constructed from studies of submarine cables Buckham *et al.* (2003) and validated in Lambert *et al.* (2003). The following model was described to have aeronautical applicability in several works, for example, in the references Coulombe-Pontbriand (2005); Howard (2007); Nahon *et al.* (2002) and Azevedo *et al.* (2013).

The cable is discretized into a series of elastic elements with the mass elements lumped at the node, capable of deforming in the axial direction, as illustrated in Fig. 2. The first node is considered to be always attached to point O, while the last node is fixed at the center mass of the vehicle.

Internal forces are generated from the cable elastic behavior. The internal elastic tension is assumed to be linear with strain, acting only at the axial direction, being for the *j*-th cable element:

$$T^j = EA_T\epsilon^j \tag{12}$$

where T^j is the elastic tension, E is the effective Young's modulus, A_T is the segment cross section and ϵ^j is the strain for that element given by:

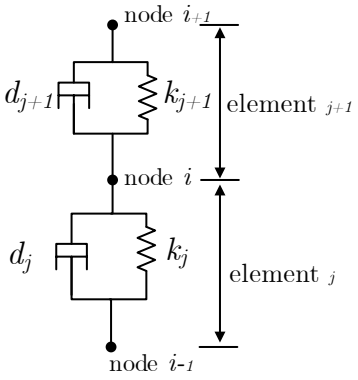

Figura 2: Elements and nodes of the tether.

$$\epsilon^j = \frac{l_s^j - l_u^j}{l_u^j} \tag{13}$$

where l_s^j corresponds to the stretched length while l_u^j corresponds to the unstretched length.

Internal damping forces were also considered, being linearly dependent with the tether element velocity, given by:

$$P^j = d_j \dot{r}^j_{Z_T} \tag{14}$$

where d_j is the damping coefficient and $\dot{r}^j_{Z_T}$ is the velocity of the j-th element.

The elements are also subjected to external disturbances, namely: aerodynamic drag and its weight. Aerodynamic drag components in *j*-th element are given by Buckham *et al.* (2003):

$$D^j_{X_\mathrm{T}} = -\frac{1}{2}\rho_{air} C_d d_c l_u^j f_p |\dot{r}_a^j|^2 \frac{\dot{r}^j_{a,X_\mathrm{T}}}{\sqrt{(\dot{r}^j_{a,X_\mathrm{T}})^2 + (\dot{r}^j_{a,Y_\mathrm{T}})^2}} \tag{15}$$

$$D^j_{Y_\mathrm{T}} = -\frac{1}{2}\rho_{air} C_d d_c l_u^j f_p |\dot{r}_a^j|^2 \frac{\dot{r}^j_{a,Y_\mathrm{T}}}{\sqrt{(\dot{r}^j_{a,X_\mathrm{T}})^2 + (\dot{r}^j_{a,Y_\mathrm{T}})^2}} \tag{16}$$

$$D^j_{Y_\mathrm{T}} = -\frac{1}{2}\mathrm{signal}(v^j_{a,q})\rho_{air} C_d d_c l_u^j f_q |\dot{r}_a^j|^2 \tag{17}$$

where ρ_{air} is the air density, C_d the tether drag coefficient,d_c is the diameter of the cable and $\dot{r}_a^j$ is the relative velocity between the wind and the center of the tether element. f_p and f_q are load functions that accounts for the non-linear breakup of drag between the tangential and normal direction and they are obtained from Azevedo *et al.* (2013).

The weight of each element is evaluted by product of the tether linear density by its unstretched length times the local acceleration of gravity.

The mass matrix for a given tether element, written in the tether's referencial, is given by:

$$\mathbf{M}^j_\mathrm{T} = \begin{bmatrix} m^j & 0 & 0 \\ 0 & m^j & 0 \\ 0 & 0 & m^j \end{bmatrix} \tag{18}$$

where m^j is mass of the element.

In ordem to solve Newton's second law for each node of the cable it is necessary to convert all forces evaluted to the inertial system. Also, the mass matrix must be written in the inertial system. Considering that half of the mass of each element that is attached to a node composes the node's mass, this expression is given in the inertial system by:

$$\mathbf{M}^i_\mathrm{I} = \frac{1}{2}\mathbf{R}^{(j+1)}_\mathrm{IT}\mathbf{M}^{(j+1)}_\mathrm{T}\mathbf{R}^{(j+1)T}_\mathrm{IT} + \frac{1}{2}\mathbf{R}^{(j)}_\mathrm{IT}\mathbf{M}^{(j)}_\mathrm{T}\mathbf{R}^{(j)T}_\mathrm{IT} \tag{19}$$

where $\mathbf{R}_{\mathrm{IT}}^{(j)}$ is the rotation matrix that transforms from the tether system to the inertial system.

Applying Newton's second law and solving for each node, one obtains:

$$\mathbf{M}_{\mathrm{I}}^{i}\ddot{\mathbf{r}}^{i} = (\mathbf{T}^{i+1} + \mathbf{P}^{i+1}) - (\mathbf{T}^{i} + \mathbf{P}^{i}) + \frac{1}{2}(\mathbf{D}^{i+1} + \mathbf{D}^{i} + m^{i+1}\mathbf{g} + m^{i}\mathbf{g}) \tag{20}$$

The parameters values that have been used in this study for simulation purposes are listed in Table 2.

Tabela 2: Parameters of the tether model.

	Parameter	Value	Units
Diameter	d_c	$10e^{-3}$	m
Linear density	λ	$28e^{-3}$	Kg/m
Young modulus	E	2	GPa
Damping coefficient	d_j	650	Kg/s
Drag coefficient	C_d	0.98	
Tether length	L	10	m

The resultant force vector of the interaction tether-multicopter, for o CM represented *n* is given by:

$$\mathbf{F}_{\mathrm{T}} = -(\mathbf{T}^{n} + \mathbf{P}^{n} - \mathbf{D}^{n} - m^{n}\mathbf{g}) \tag{21}$$

3. CONTROL SYSTEM

The multicopter control strategy presented in this section is described by Santos *et al.* (2013). Let us define the total thrust vector $\in \mathbb{R}^3$ of the octocopter to be:

$$\mathbf{f} \triangleq f\mathbf{n}. \tag{22}$$

Let us define the inclination angle $\varphi \in \mathbb{R}$ of the octocopter to be:

$$\varphi \triangleq \cos^{-1} n_z. \tag{23}$$

Note that φ consists of the angle between $\mathbf{n}$ and Z_{R} (see Figure 3).

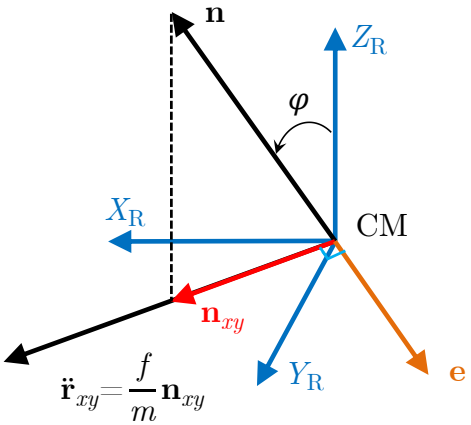

Figura 3: Relationship between the normal unit vector $\mathbf{n}$ and the horizontal acceleration $\ddot{\mathbf{r}}_{xy}$.

Let $\bar{\mathbf{r}} \triangleq [\bar{r}_x\ \bar{r}_y\ \bar{r}_z]^{\mathrm{T}} \in \mathbb{R}^3$ denote the position desired for the octocopter and define the corresponding tracking error $\tilde{\mathbf{r}}^{(i)} \in \mathbb{R}^3$ by

$$\tilde{\mathbf{r}} \triangleq \mathbf{r} - \bar{\mathbf{r}}. \tag{24}$$

Let $\varphi_{\max} \in \mathbb{R}$ be the maximum allowable values of the inclination angle φ, $f_{\min} \in \mathbb{R}$ and $f_{\max} \in \mathbb{R}$ be, respectively, the minimum and the maximum allowable values of the total thrust magnitude f. The solution to the problem of position control is to find a feedback control law for $\mathbf{f}$, which make $\mathbf{r} \to \bar{\mathbf{r}}$ or $\tilde{\mathbf{r}} \to \mathbf{0}$, while respecting the constraints $f_{\min} \leq f \leq f_{\max}$ and $\varphi \leq \varphi_{\max}$. The control position is partitioned into control height and horizontal position control.

3.1 Height Control

From Equation (10), the dynamic model of the height of the vehicle r_z is given by

$$\ddot{r}_z = \frac{n_z}{m} f - g. \tag{25}$$

Consider the system modeled by Equation (25), and the minimum $f_{\min} > 0$ and maximum $f_{\max} > f_{\min}$ allowable values of the command total thrust magnitude f. Assume that m, g and $n_z \neq 0$ are exactly known. The feedback control law is given by:

$$f = \begin{cases} f_{\min}, & \alpha_z < f_{\min} \\ \alpha_z, & \alpha_z \in [f_{\min}, f_{\max}] \\ f_{\max}, & \alpha_z > f_{\max} \end{cases} \tag{26}$$

with

$$\alpha_z \triangleq \frac{m}{n_z} \left(g - k_1 \left(r_z - r_{\mathrm{z}} \right) - k_2 \dot{r}_z \right), \tag{27}$$

respecting the total thrust magnitude constraint $f_{\min} \leq f \leq f_{\max}$ and is such that if $f_{\min} \leq \alpha_z \leq f_{\max}$, then the vehicle height r_z responds to the height desired $\overline{r}_z$, as if it were governed by the following second order linear time-invariant (LTI) system:

$$\ddot{r}_z + k_2 \dot{r}_z + k_1 r_z = k_1 \overline{r}_z, \tag{28}$$

where $k_1 > 0 \in \mathbb{R}$ e $k_2 > 0 \in \mathbb{R}$ are controller coefficients.

3.2 Horizontal Position Control

Let $\mathbf{r}_{xy} \triangleq [r_x \; r_y]^{\mathrm{T}} \in \mathbb{R}^2$ and $\mathbf{n}_{xy} \triangleq [n_x \; n_y]^{\mathrm{T}} \in \mathbb{R}^2$ denote the horizontal projections of $\mathbf{r}$ and $\mathbf{n}$, respectively. From equation (10), one can write the horizon position dynamic model as

$$\ddot{\mathbf{r}}_{xy} = \frac{f}{m} \mathbf{n}_{xy}. \tag{29}$$

Consider the system modeled by equation (29) and the maximum allowable value $\varphi_{\max} > 0$ of the inclination angle φ. Assume that m and $f \neq 0$ are exactly known. The feedback control law is given by:

$$\mathbf{n}_{xy} = \begin{cases} \boldsymbol{\alpha}_{xy}, & \|\boldsymbol{\alpha}_{xy}\| \leq \sin\varphi_{\max} \\ \sin\varphi_{\max} \frac{\boldsymbol{\alpha}_{xy}}{\|\boldsymbol{\alpha}_{xy}\|}, & \|\boldsymbol{\alpha}_{xy}\| > \sin\varphi_{\max} \end{cases}, \tag{30}$$

with

$$\boldsymbol{\alpha}_{xy} \triangleq -\frac{m}{f} \left[k_z \left(\mathbf{r}_{xy} - \mathbf{r}_{xy} \right) + k_4 \dot{\mathbf{r}}_{xy} \right], \tag{31}$$

respecting the inclination angle constraint $\varphi \leq \varphi_{\max}$ and is such that if $\|\boldsymbol{\alpha}_{xy}\| \leq \sin\varphi_{\max}$, then $\mathbf{r}_{xy}$ responds to the horizontal position desired $\overline{\mathbf{r}}_{xy} \triangleq [\overline{r}_x \; \overline{r}_y]^{\mathrm{T}}$ as if it were governed by the following pair of second order LTI systems:

$$\ddot{\mathbf{r}}_{xy} + k_4 \dot{\mathbf{r}}_{xy} + k_3 \mathbf{r}_{xy} = k_3 \overline{\mathbf{r}}_{xy}, \tag{32}$$

where $k_3 > 0 \in \mathbb{R}$ e $k_4 > 0 \in \mathbb{R}$ are controller coefficients.

In practice, the attitude desired for the internal attitude control loops need to be computed from the normal unit vectors $\mathbf{n}$. In order to specify a unique attitude, it is necessary to select a heading. For example, one can choose a zero heading just by taking into consideration the attitude represented by the principal Euler angle/axis $(\varphi, \mathbf{e})$, where φ is the angle of inclination own and $\mathbf{e} \in \mathbb{R}^3$ is a unit vector (see Figure 3) is given by:

$$\mathbf{e} = \frac{\mathbf{n} \times \mathbf{n}_{xy}}{\|\mathbf{n} \times \mathbf{n}_{xy}\|} \tag{33}$$

From $(\varphi, \mathbf{e})$ one can thus represent the attitude of S_{B} with respect to S_{R}, using , for example, Euler angles parameterization that permits obtains $\overline{\phi}$, $\overline{\theta}$ and $\overline{\psi}$.

4. SIMULATION RESULTS

The multicopter dynamics is integrated by using the fourth order Runge-Kutta method with time step of T = 0.002 s. The initial position is $\mathbf{r}_i = [0\ 0\ 0]^{\mathrm{T}}$m. The mass of vehicle is $m = 2.132$ kg and the gravity acceleration is $g = 9.796$ m/s^2. The control parameters of vehicle, k_1, k_2, k_3 and k_4, are chosen based on equations (28) and (32). The maximum overshoot of $M_{\mathrm{p}}^{\mathrm{ref}} = 0.02$ m, and a peak time of $t_{\mathrm{p}}^{\mathrm{ref}} = 2$ s, were selected, which resulted in $k_1 = 6.29$ and $k_2 = 3.91$. Similarly, the maximum overshoot of $M_{\mathrm{p}}^{\mathrm{ref}} = 0.02$ m and a peak time of $t_{\mathrm{p}}^{\mathrm{ref}} = 3$ s were selected and the $k_3 = 2.78$ and $k_4 = 2.61$ gains were obtained. The proportional gain tether control selected was k_p = 0.01. The simulation was ran for 10 seconds, and the following bounds were selected: φ_{max} = 30°, f_{max} = 40 N e f_{min} = 2 N.

The vehicle was commanded to the hover position in $\mathbf{r} = [0\ 0\ 10]^{\mathrm{T}}$m and simultaneously a wind disturbance was added in the direction of the X axis. The disturbance has a sinusoidal shape with amplitude range 3,5,7,9[m/s] and constant frequency of 0.5 [Hz]. Four different scenarios were evaluated with the aforementioned wind velocities.

The simulations provided a comparison between free and tethered flight. The control error was quantified by the root mean square error, given by:

$$\mathrm{E}^{\mathrm{RMS}} = \sqrt{\frac{1}{3}[(\text{error x})^2 + (\text{error y})^2 + (\text{error z})^2]}. \tag{34}$$

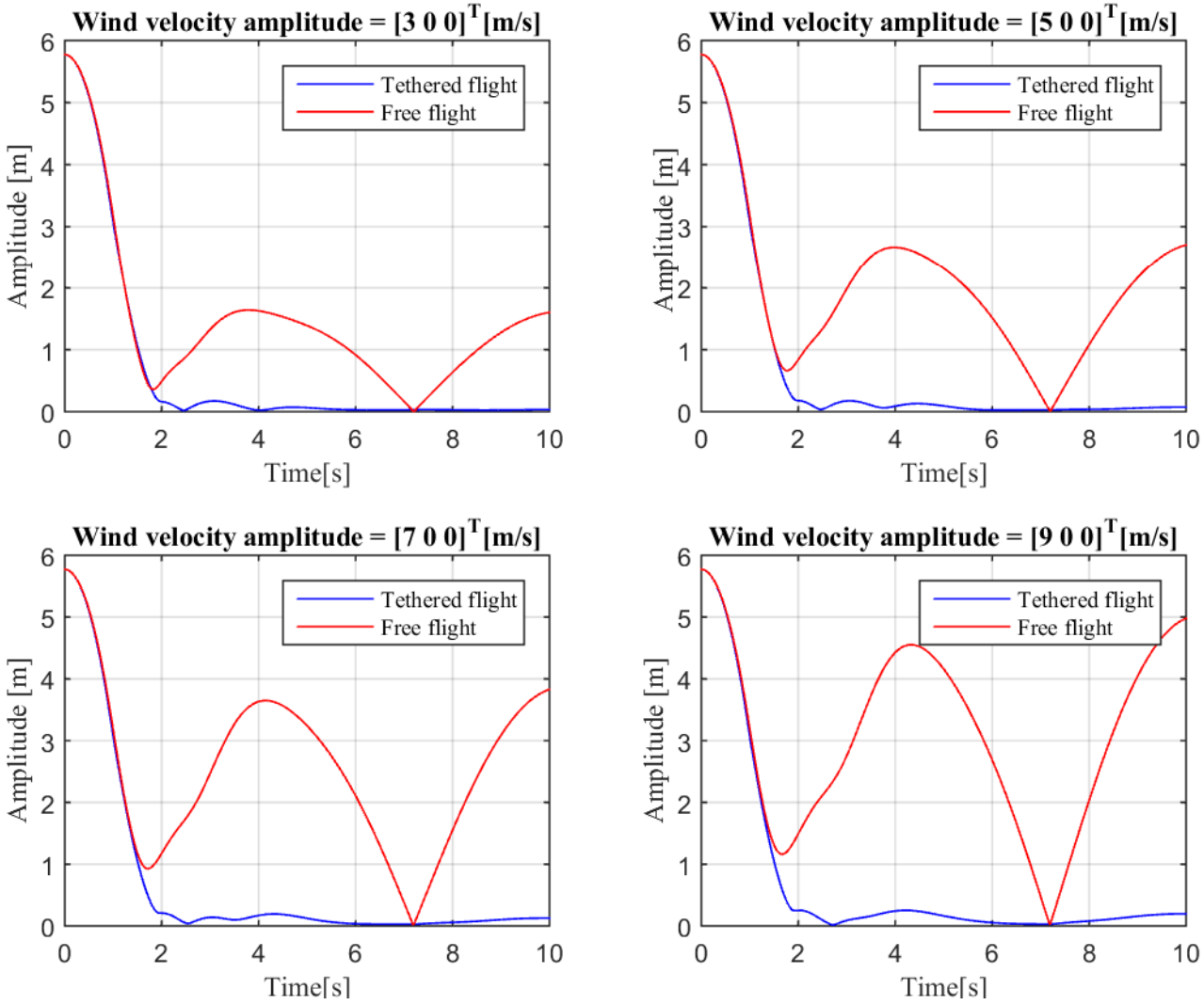

Figura 4: Root mean square error for different wind velocities.

Figure 4 presents the position tracking error of the hover flight. We can note that the greater the disturbance amplitude is, the greater will be the control error for the free flight vehicle. On the other hand, the tethered vehicle seems to be less sensitive to the variation of the perturbation.

Figure 5 presents the geometry of the tether using 9 nodes. To obtain this image it was applied a constant wind velocity disturbance to the vehicle. It is evident that increasing the wind velocity the catenary-like shape of the tether is more apparent. Moreover, we can note that the position of the last node lowers along the Z_{I} axis as the velocity increases.

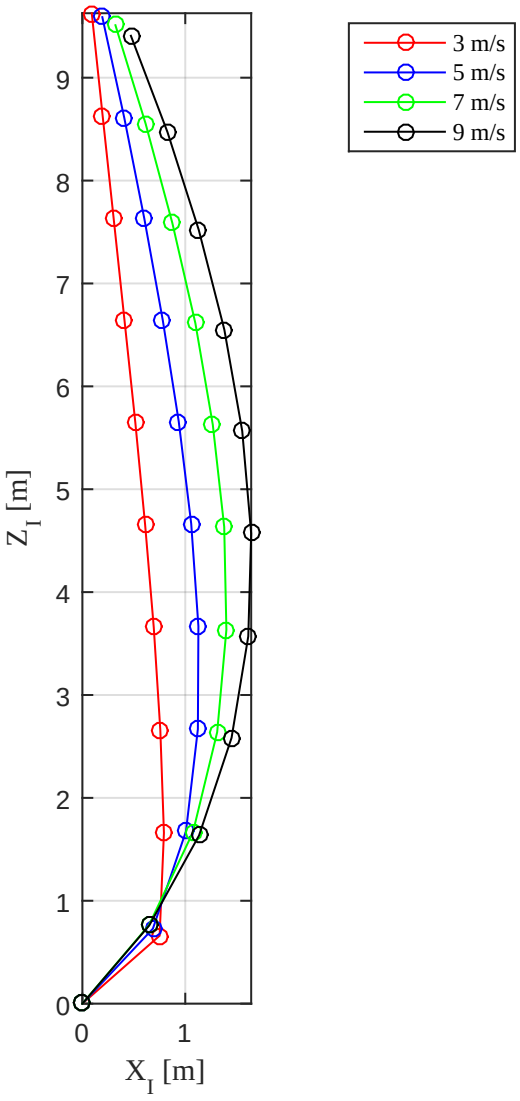

Figura 5: Geometry of the tether for 9 nodes.

5. CONCLUSIONS

This work has presented the modeling and control of a tethered MAV configuration. Numerical simulations showed that, when compared with the traditional vehicle in free flight, the tethered configuration has a better performance under external disturbances. The tether reduces the position error amplitude, improving the robustness of the vehicle. For future work, we consider an improved aerodynamic model for the vehicle, the control design for the tether tension and a pertubation model that corresponds to actual wind profiles in outdoor environments.

6. ACKNOWLOGEMENTS

The authors thank Coordenação de Aperfeiçoamento de Pessoal de Nível Superior (CAPES) and Conselho Nacional de Desenvolvimento Científico e Tecnológico (CNPq) for financial supports.

7. REFERENCES

Azevedo, B.A., de O. Cunha, M., Morales, M., Góes, L.C.S. and Paglione, P., 2013. "Stability and Active Control of Low Altitude Aerostats". AIAA Lighter-Than-Air Systems Technology (LTA) Conference, p. 1299.

Buckham, B., Nahon, M., Seto, M., Lambert, C. and Zhao, X., 2003. "Dynamics and control of a towed underwater vehicle system, part I: Model development". *Ocean Engineering*, Vol. 30, p. 453–470.

Castro, D.F., Prado, I.A.A., de Freitas Virgílio Pereira, M., dos Santos, D.A. and Balthazar, J.M., 2016. "Modeling and Position Control of Tethered Octocopters". Submitted to International Conference on Structural Nonlinear Dynamics and Diagnosis (CSNDD'2016).

Castro, D.F., Santos, J.S., Oliveira, M.B.X., Santos, D.A. and Góes, L.C.S., 2015. "Modeling and Control of Tethered Unmanned Multicopters in Hovering Flight". AIAA Aviation, Dallas,USA.

Coulombe-Pontbriand, P., 2005. *Modeling and Experimental Characterization of a Tethered Spherical Aerostat*. Master's thesis, McGill University (Canada).

Howard, A.J.G., 2007. *Experimental Characterization and Simulation of a Tethered Aerostat with Controllable Tail Fins*. Master's thesis, McGill University (Canada).

Khaleefa, S., Alsamhi, S. and Rajput, N., 2014. "Tethered balloon technology for telecommunication, coverage and path loss". IEEE Students Conference on Electrical, Electronics and Computer Science.

Lambert, C., Nahon, M., Buckham, B. and Seto, M., 2003. "Dynamics and control of a towed underwater vehicle system, part II: Model validation and turn maneuver optimization". *Ocean Engineering*, Vol. 30, pp. 471–485.

Nahon, M., Gilardi, G. and Lambert, C., 2002. "Dynamics/Control of a Radio Telescope Receiver Supported by a Tethered Aerostat". *Journal of Guidance, Control and Dynamics*, Vol. 25, No. 6, pp. 1107–1115.

Nohmi, M., 2009. "Mission design of a tethered robot satellite stars for orbital experiment". 18th IEEE International Conference on Control Applications.

Papachristos, C. and Tzes, A., 2014. "The power tethered uav ugv team: A collaborative strategy for navigation in partially mapped environments". 22nd Mediterranean Conference on Control and Automation (MED).

Rye, D., 1985. "Longitudinal stability of a hovering tethered rotorcraft". *Journal of Guindance, Control and Dynamics*, Vol. 8, pp. 743–752.

Sandino, L.A., Bejar, M., Kondak, K. and Ollero, A., 2013a. "Improving hovering performance of tethered unmanned helicopters with nonlinear control strategies". Proceedings of the International Conference on Unmanned Aircraft Systems, p. 443–452.

Sandino, L.A., Bejar, M., Kondak, K. and Ollero, A., 2013b. "On the use of tethered configurations for augmenting hovering stability in small-size autonomous helicopters". *Journal of Intelligent and Robotic Systems*, Vol. 70, p. 509–525.

Sandino, L.A., Bejar, M., Kondak, K. and Ollero, A., 2014. "Advances in Modeling and Control of Tethered Unmanned Helicopters to Enhance Hovering Performance". *Journal of Intelligent and Robotic Systems*, Vol. 73, pp. 3–18.

Santos, D.A., Saotome, O. and Cela, A., 2013. "Trajectory control of multirotor helicopters with thrust vector constraints". IEEE 21st Mediterranean Conference on Control and Automation, Chania, Greece.

Schmidt, G. and Swik, R., 1974. "Automatic hover control of an unmanned tethered rotoplatform". *Automatica*, Vol. 10, pp. 393–403.

Wertz, J.R., 1978. *Spacecraft Attitude Determination and control*. Kluwer Academic Publishers, The Netherlands.

8. RESPONSABILITY NOTICE

The authors are the only responsible for the printed material included in this paper.